

STAR FORMATION HISTORY AND EXTINCTION IN THE CENTRAL KILOPARSEC OF M82-LIKE STARBURSTS

Y. D. MAYYA,¹ A. BRESSAN,^{2,3} M. RODRÍGUEZ,¹ J. R. VALDES,^{1,2} AND M. CHAVEZ^{1,4}

Received 2003 June 22; accepted 2003 September 5

ABSTRACT

We report on the star formation histories and extinction in the central kiloparsec region of a sample of starburst galaxies that have similar far-infrared (FIR), 10 μm , and K -band luminosities as those of the archetype starburst M82. Our study is based on new optical spectra and previously published K -band photometric data, both sampling the same area around the nucleus. Model starburst spectra were synthesized as a combination of stellar populations of distinct ages formed over the Hubble time and were fitted to the observed optical spectra and K -band flux. The model is able to reproduce simultaneously the equivalent widths of emission and absorption lines, the continuum fluxes between 3500 and 7000 \AA , and the K -band and FIR flux. A good fit requires a minimum of three populations: (1) a young population of age ≤ 8 Myr, with its corresponding nebular emission, (2) an intermediate-age population (age < 500 Myr), and (3) an old population that forms part of the underlying disk or/and bulge population. The birthrate parameter, which is defined as the ratio of the current star formation rate to the average past rate, is found to be in the range 1–12. The contribution of the old population to the K -band luminosity depends on the birthrate parameter and remains above 60% in the majority of the sample galaxies. Even in the blue band, the intermediate-age and old populations contribute more than 40% of the total flux in all the cases. A relatively high contribution from the old stars to the K -band nuclear flux is also apparent from the strength of the 4000 \AA break and the Ca II K line. The extinction of the old population is found to be around half that of the young population. The contribution to the continuum from the relatively old stars has the effect of diluting the emission equivalent widths below the values expected for young bursts. The mean dilution factors are found to be 5 and 3 for the H α and H β lines, respectively.

Subject headings: dust, extinction — galaxies: starburst — stars: formation

On-line material: color figures

1. INTRODUCTION

Starburst galaxies harbor thousands of massive stars that are responsible for their typical nebular spectra and high far-infrared (FIR) emission (Weedman et al. 1981). Massive stars are short-lived, typically less than 10 Myr; consequently, most of the derived properties of the starburst regions pertain to the last generation of massive stars. On the other hand, starburst galaxies have potential to form stars for periods much longer than this. For example, M82, the prototype of a starburst, has a sufficient amount of gas to sustain star formation for a few hundreds of million years (Walter, Weiss, & Scoville 2002). But does the star formation really continue for periods much longer than the typical age of massive stars? By their very nature, studies based on emission lines are unable to answer this question. We need techniques that use tracers of lower mass stars, which live for several tens or even a few hundreds of million years.

The optical spectra of these older stellar systems are characterized by prominent Balmer absorption lines. Indeed, Kim et al. (1995) found such absorption lines to be common in starburst spectra. In recent years, there have been attempts to

use the information contained in the absorption lines to derive the properties of one or more assumed older bursts in individual galaxies, e.g., NGC 7714 (Lançon et al. 2001) and NGC 7679 (Gu et al. 2001). Stellar populations a few hundreds of million years old have been inferred in these studies. However, these stellar features are not being routinely used to derive properties, such as the age and mass of the older stellar populations, of a representative sample of galaxies. This is probably because of difficulties in analyzing the absorption features in the presence of nebular emission. Recently, Poggianti, Bressan, & Franceschini (2001) have developed a technique based on synthetic spectra that allows investigation of many previous bursts simultaneously. Their technique is capable of handling Balmer emission lines even in the presence of an underlying absorption line, and vice versa, and hence is ideal for an analysis of the complete star formation history of starburst regions.

The star formation history of a starburst nucleus depends on the spatial scale under investigation. Observations of nearby starburst galaxies with the *Hubble Space Telescope* have resolved starburst nuclei into several tens or, in some cases, a few hundreds of compact clusters known as super-star clusters (SSCs; O’Connell et al. 1995). SSCs show a considerable range in their colors, suggesting a spread in their ages. Typically, SSCs are found in a region within a few hundred parsecs of the starburst nucleus. In M82, regions with strong Balmer absorption lines are found as far as 1 kpc from the currently active starburst site (O’Connell & Mangano 1978). If we were to place M82 at the distance of Arp 220, an ultraluminous far-infrared galaxy, all the regions discussed

¹ Instituto Nacional de Astrofísica, Óptica y Electrónica, Luis Enrique Erro 1, Tonantzintla, Apartado Postal 51 y 216, C.P. 72840, Puebla, Mexico; ydm@inaoep.mx, mrodri@inaoep.mx, jvaldes@inaoep.mx, mchavez@inaoep.mx.

² Osservatorio Astronomico di Padova, Vicolo dell’Osservatorio 535122, Padua, Italy; bressan@pd.astro.it.

³ Scuola Internazionale Superiore di Studi Avanzati, Via Beirut 4, I-34014 Trieste, Italy.

⁴ Currently at LPL and Steward Observatory, University of Arizona, Tucson, AZ 85719.

above would be inside an aperture of $3''$. Thus, ground-based spectra of distant starburst nuclei would include not only the present burst but also the outlying older bursts, if any. Therefore, we need to study the star formation history of nearby starburst nuclei over a spatial scale of ~ 1 kpc in order to compare the results with those of distant galaxies.

Star-forming regions are always associated with dust, which has the effect of reddening the observed spectrum. The amount of reddening is traditionally determined by comparing the observed Balmer emission line ratios with theoretical values (Osterbrock 1989) and making use of the Galactic reddening curve (Cardelli, Clayton, & Mathis 1989). An alternative method to find the reddening is to compare the observed ultraviolet continuum slope of the star-forming regions with that expected for young starbursts from synthetic models (Fanelli, O'Connell, & Thuan 1988). Using the above two techniques, it is now well established that the reddening suffered by the emission lines in starburst regions is significantly higher than the reddening suffered by the continuum (Fanelli et al. 1988; Calzetti, Kinney, & Storchi-Bergmann 1994). The difference in the reddening is understood to be due to the escape of stars from the parent molecular clouds as they get older (Calzetti et al. 1994; Silva et al. 1998). Calzetti et al. (1994) also found that the mean attenuation curve toward the starburst regions is grayer than that of the Milky Way. Charlot & Fall (2000) investigated these issues in detail and concluded that a key ingredient that is responsible for a differential reddening between lines and continuum and a gray reddening curve, is the finite lifetime of the stellar birth clouds. Granato et al. (2001) found that the starburst spectra could be modeled even by using the Galactic reddening curve, when each stellar population constituting the starburst is allowed to have its own extinction. It is important to note that the low observed strength of the 2200 Å ultraviolet bump in starburst spectra could also be produced by the models of Granato et al.

In this work, we study the star formation histories of the central kiloparsec region of a sample of starburst galaxies, focusing on determining the masses of all the stellar populations that contribute to the optical spectrum. The relative contributions of the young and old populations to the K -band flux are also determined. We use the entire optical spectrum, not just a few emission and absorption lines, so that our observables are sensitive not only to the young burst but also to all the previous bursts. The starburst model of Poggianti et al. (2001) is used. The extinction of each population is a free parameter to be evaluated by the fitting procedure. In § 2, we describe the sample and observations. The starburst model is explained in § 3. The star formation history of the sample galaxies is discussed in § 4. Concluding remarks are given in § 5.

2. SAMPLE, OBSERVATIONS, AND ANALYSIS

Devereux (1989) defined a complete sample of *nearby starburst galaxies* that includes all nearby, $16 \leq D(\text{Mpc}) \leq 40$ (Hubble constant of $75 \text{ km s}^{-1} \text{ Mpc}^{-1}$), non-Seyfert 1 galaxies with central $10 \mu\text{m}$ luminosity $\geq 6 \times 10^8 L_{\odot}$, declination $-35^{\circ} \leq \delta \leq +60^{\circ}$, right ascension $22^{\text{h}} \leq \alpha \leq 16^{\text{h}}$, and Galactic latitude $b \geq 20^{\circ}$. The sample contains 20 galaxies, whose K -band and FIR luminosities are very similar to those of the prototypical starburst M82. The FIR luminosities, as estimated from 60 and $100 \mu\text{m}$ *Infrared Astronomical Satellite* (*IRAS*) fluxes, lie between 10^{10} and $10^{11} L_{\odot}$, which are intermediate between those of normal galaxies and

ultraluminous far-infrared galaxies. We carried out long-slit optical spectrophotometry of 12 of these galaxies at the Guillermo Haro Astrophysical Observatory, Cananea, Mexico, during two observing runs in 1999 February and December. A grating with $150 \text{ lines mm}^{-1}$ was used, which resulted in a resolution of about 10 \AA and a spectral coverage of $\approx 3500\text{--}6800 \text{ \AA}$. The spectral and spatial samplings were $3.2 \text{ \AA pixel}^{-1}$ and $0''.46 \text{ pixel}^{-1}$, respectively. Slit widths were typically of $1''.6$, centered on the starburst nucleus. The slit was aligned along the east-west direction for the sample galaxies. The objects were observed as close to the meridian as possible, with maximum air mass of ≈ 1.30 . Two spectra of 30 minutes each were taken for each galaxy. The instrumental response was calibrated by the observation of the standard stars HR 1544, HR 5501, BD +40°4032, Feige 15, and Feige 34.

Each frame was bias-corrected and divided by a normalized flat field, using various tasks in the IRAF package. Two wavelength-calibrated frames of the same galaxy were averaged, in the process removing cosmic-ray events. Sky spectra were extracted from the object-free regions of the long slit and subtracted from each starburst spectrum. The spectra of the sample starbursts were extracted over a slit length of $9''$, which corresponds to physical scales of $0.77\text{--}1.76$ kpc. The average signal-to-noise ratios of the extracted spectra are ≈ 50 and 20 around 5500 and 3700 \AA , respectively. We estimate that the spectrophotometry is accurate to better than 10% over the entire wavelength range covered.

The general properties of the observed starburst nuclei are presented in Table 1. The Hubble types and distances to the galaxies are given in columns (2) and (3), respectively. The distances are based on the recessional velocities in the Nearby Galaxy Catalog (Tully 1988). Column (4) contains the FIR luminosity (L_{FIR}), which was calculated from the 60 and $100 \mu\text{m}$ *IRAS* fluxes (Helou et al. 1988). *IRAS* beams, in general, enclose the entire galaxy, and hence a part of the *IRAS* flux could originate in regions outside the nucleus. However, recent high-resolution mid-infrared images of starburst galaxies obtained with the *Infrared Space Observatory* show that most of the *IRAS* flux originates within a spatial scale of around 1 kpc (Förster-Schreiber et al. 2003), which is the slit length used for the extraction of spectra of our sample galaxies. We estimated the V -band magnitudes in an aperture of $9''$ (V_{ap}), using the compilation of multiaperture photometric data by Prugniel & Héraudeau (1998). These magnitudes are tabulated in column (5). V -band magnitudes were also obtained from our slit spectra (V_{sp}). The two magnitudes were measured with the specific purpose of providing two approximate limits on the ratio between FIR and V -band luminosity (FIR/V). The FIR/V ratios using the aperture and slit V -band fluxes are given in columns (6) and (7), respectively [$\text{FIR}/V = L_{\text{FIR}}/(L_{5500,5500})$, where L_{5500} is the monochromatic luminosity in the V band]. For compact sources, the real values are expected to be close to FIR/V_{sp} , whereas for extended sources, they may be as low as FIR/V_{ap} . The K -band flux inside our slit (see § 3.3), normalized to the slit V -band flux, is given in column (8). Column (9) contains the $B\text{--}V$ color obtained from the extracted spectra. The visual extinction (A_V) and the gas metallicity Z are given in columns (10) and (11), respectively.

The value of A_V was obtained by comparing the ratio of $\text{H}\alpha$ to $\text{H}\beta$ to its case B value, making use of the Galactic extinction curve (Osterbrock 1989). However, the measurement of A_V in the presence of underlying absorption is not trivial (Rosa-González, Terlevich, & Terlevich 2002). The measured values

TABLE 1
GENERAL PROPERTIES OF THE SAMPLE STARBURST NUCLEI

NGC (1)	Type (RC3) (2)	Distance (Mpc) (3)	$L_{\text{FIR}}^{\text{b}}$ (4)	m_V^{a} (mag) (5)	FIR/V_{ap} (6)	FIR/V_{sp} (7)	F_K/F_V (8)	$B-V$ (mag) (9)	A_V (mag) (10)	Z/Z_{\odot} (11)
470.....	Sb	30.50	10.13	14.65	16.62	37.73	0.39	0.83	2.31	3.95
1022.....	SBa	18.50	10.13	14.15	28.82	100.84	0.31	0.70	3.32	2.91
2273.....	SBa	28.40	10.03	13.95	6.84	16.42	0.35	1.02	3.74	0.20
2750.....	SABc	38.40	10.17	14.15	7.12	24.47	0.19	0.39	2.84	2.37
2782.....	SABa	37.30	10.39	13.92	10.84	19.19	0.26	0.56	2.04	1.49
3504.....	SABab	26.50	10.47	13.10	11.04	23.50	0.24	0.60	3.30	2.40
4102.....	SABb	17.00	10.44	13.00	25.00	56.75	0.49	1.03	5.25	0.43
4194.....	IBm	39.10	10.82	13.55	18.63	44.27	0.24	0.48	3.02	1.17
4273.....	SBc	35.10	10.49	14.10	17.53	67.90	0.21	0.66	2.69	2.96
4385.....	SB0	33.50	10.01	14.45	8.77	17.82	0.16	0.30	1.17	2.40
4818.....	SABab	21.50	10.26	13.41	13.77	78.52	0.55	1.05	4.65	3.51
4984.....	SAB0	21.30	10.01	12.80	4.19	26.42	0.59	1.00	3.53	1.98

^a V -band magnitude in 9'' aperture.

^b Luminosities in $\log(L/L_{\odot})$ units.

are somewhat sensitive to the assumed values of the equivalent widths (EWs) of the underlying absorption lines, and this can increase the uncertainty in Z . McCall, Rybski, & Shields (1985) demonstrated that the stellar absorption correction and extinction for each galaxy could be estimated if the $\text{H}\gamma$ line is detected in emission. They recommended a mean absorption correction of 2 Å to the EWs of the first three lines in Balmer series. However, the $\text{H}\gamma$ emission line is not seen in five of the sample galaxies. Hence, we cannot follow the method used by McCall et al. (1985) uniformly for all the galaxies. Alternatively, we followed an iterative method to obtain the best estimate of A_V . First, we used the observed spectra with a 2 Å correction to the Balmer EWs, to make a preliminary estimation of the nebular abundances. Then the entire spectral fitting analysis, described in detail in § 3.1, was carried out using these abundances. We then measured the visual extinction on the resulting young population model component. This component is not affected by the underlying line absorption arising from the intermediate-age populations. The abundance measurement was refined using this new value of the extinction. The strong-line method was used to derive the oxygen abundance from the observed nebular lines using the calibration of McCall et al. (1985). The oxygen abundance was converted to metallicity in solar units by assuming that $12 + \log(\text{O}/\text{H}) = 8.74$ for the Sun (Holweger 2001).

3. THE THEORETICAL ANALYSIS

In principle, the analysis of the EW of the hydrogen emission lines (e.g., $\text{H}\beta$) provides information on the age of the most recent burst of star formation (Leitherer et al. 1999), and the Balmer decrement gives the extinction values. However, as discussed in the introduction, a typical slit may enclose several stellar populations of different ages and a complex distribution of dust. Thus, in practice, the EW method is heavily affected by the uncertainty concerning the contributions of intermediate-age and old populations to the continuum (and even line absorption) below the emission lines.

On the other hand, the observed spectral energy distributions (SEDs) contain much more information than can be derived from a simple application of the Balmer decrement method and EW analysis. The physical insight can be even

greater if one uses the *IRAS* fluxes and K -band photometry. The FIR emission provides a strong constraint on the current star formation rate (SFR), although the difference in aperture sizes between the *IRAS* data and our spectra may constitute a serious problem. As for the nuclear K -band luminosity, there is a debate as to whether it originates from the old population or is provided by red supergiant stars associated with the recent star formation history (see § 4.2). In order to obtain a complete picture of star formation and extinction in starburst galaxies, we have analyzed the SEDs by means of the population synthesis technique.

3.1. The Starburst Model

The technique adopted to model the observed spectra is an improved version of that described by Poggianti et al. (2001). The star formation history over the Hubble time is broken up into several episodes. Each episode is described by a burst of star formation, whose rate is constant over a certain period of time. Evolution of the spectra within a single episode is assumed to be negligible, and hence each episode is represented by an SED of a simple stellar population (SSP). An SSP is characterized by age and metallicity. The ages of SSPs are suitably selected to provide the main spectral characteristics seen in starburst spectra (emission and absorption features and the overall continuum) and are combined with appropriate intensity and extinction.

We used nine SSPs, eight of them formed over the last 1 Gyr, while the ninth one represents the underlying old population. Ages of the first eight SSPs are 2, 7, 10, 50, 100, 300, 500, and 1000 Myr. The duration of each star formation episode is chosen in such a way that the SED remains representative of all the ages that are included by the episode. The resulting durations are 4, 4, 7, 60, 125, 200, 350, and 1250 Myr, respectively. We would only use these durations in the conversion between the stellar mass and the SFR. Henceforth, episodes of star formation corresponding to the first three SSPs will be referred to as the “young population,” those for the next four SSPs as the “intermediate-age population,” and the populations older than ~ 1 Gyr as the “old population.” The old population is meant to represent the sum of the bulge and disk components that enter the slit area.

For each SSP we adopt a uniform screen attenuation, using the standard extinction law for the diffuse medium in our Galaxy [$R_V = A_V/E(B - V) = 3.1$; Cardelli et al. 1989]. While a more complex picture of the extinction cannot be excluded, it was comprehensively shown by Poggianti et al. (2001) that the characteristics of the emerging spectrum require a significant amount of *foreground* dust (screen model). Indeed, in the case of a uniform mixture of dust and stars, increasing the obscuration does not yield a corresponding increase in the *reddening* of the spectrum: the latter saturates to a value $E(B - V) \sim 0.18$, which is too low to account for the observed emission line ratios (see also Calzetti et al. 1994). The extinction value A_V is allowed to vary for the different stellar populations, and the extinguished SEDs of all the single generations are added up to give the total integrated spectrum.

Allowing the extinction of each population to vary results in a degeneracy between extinction and SFR, in such a way that there can be populations with very high SFR, but completely extinguished, thus contributing insignificantly to the total SED. If the extinguished population is old, then it will not even contribute to the FIR emission. This degeneracy can increase somewhat arbitrarily the predicted mass-to-light ratio of the system. In order to avoid such extinguished populations, we automatically tested and excluded from the solution those intermediate-age and old populations that contribute less than 1% to the total flux at all wavelengths. Although dusty young populations may not contribute significantly to the optical bands, they are important contributors to the FIR emission, and hence the populations younger than 10 Myr are retained irrespective of their contribution to the total flux at any wavelength. In this way, the algorithm naturally selects not more than four SSPs. This is consistent with the time resolution of a general population synthesis technique, when one takes into account observational errors and uncertainties of the models.

Our SSPs have a Salpeter-like initial mass function (IMF)— $N(M) dM \propto M^{-2.35} dM$ —with masses between 0.15 and $120 M_\odot$. The stellar spectral atlas is that of Jacoby, Hunter, & Christian (1984), extended in the UV and near-infrared (NIR) with Kurucz (1993) models, as described in Bressan, Granato, & Silva (1998).

The young population spectrum includes the nebular spectrum, which is calculated by means of case B photo-ionization models computed with CLOUDY (Ferland 1996) using the following parameters: mass of the ionizing cluster $10^5 M_\odot$, electron number density $n = 100 \text{ cm}^{-3}$, inner radius 15 pc, and metallicity rescaled to that of the SSP. Since our main interest is to model the hydrogen spectral features (emission and absorption lines), changing these parameters would not affect our conclusions significantly.

The gas metallicity of the majority of our sample of starburst galaxies, in which the metallicity could be reliably measured, is supersolar. Possible exceptions are NGC 2273 and NGC 4102. The former galaxy is known to have a weak Seyfert component (Devereux 1989), which is possibly contaminating the [O III] $\lambda 5007$ line, thus resulting in an underestimation of its metallicity. NGC 4102 is the most extinguished galaxy of the sample, and its low metallicity could be due to a possible overcorrection to the extinction of the [O II] $\lambda 3627$ line. Thus, in general, the young populations are metal-rich. However, the metallicity of the old stars must be lower than that; in the Galactic bulge, the average value is around half-solar (Sadler, Rich, & Terndrup 1996). Thus, except for NGC 2273, we have adopted $Z = 2.5 Z_\odot$ for the

intermediate and young populations and $Z = 0.5 Z_\odot$ for the old population. For NGC 2273, we have adopted $Z = Z_\odot$ for the young stellar populations. The results do not depend critically on the adopted metallicity.

To evaluate the best-fit model, we minimize a merit function MF, which was constructed from the EWs of H δ , H β , and H α and the relative intensities of the continuum flux in 12 almost featureless narrow spectral windows (3580–3680 Å, 3845–3880 Å, 3900–3920 Å, 4000–4060 Å, 4140–4300 Å, 4400–4600 Å, 4700–4820 Å, 5080–5180 Å, 5400–5700 Å, 5950–6200 Å, 6350–6450 Å, and 6630–6660 Å). A merit function is obtained from the differences between modeled and observed values at the selected spectral windows/features, following the definition:

$$\text{MF} = \sum_{i=1}^n \left(\frac{M_i - O_i}{E_i} W_i \right)^2, \quad (1)$$

where M_i and O_i are, respectively, the model and observed fluxes (or EWs), and E_i and W_i are the corresponding errors and weights. The errors in the spectral window were estimated as the rms fluctuations of the observed flux in the corresponding wavelength interval, while errors of EWs are expressed as a percentage value above a minimum value of 0.1, 0.1, and 1 Å, respectively, for H δ , H β , and H α . The minimization procedure applies the algorithm of adaptive simulated annealing (Ingber 1989) for a continuum multidimensional parameter space to an MF. It is important to stress that the algorithm of adaptive simulated annealing is able to avoid local minima and provides convergence to the global minimum. However, the uncertainties of the synthesis technique, combined with the observational errors, do not allow us to distinguish subpopulations within the same broad age ranges: young, intermediate, and old. For the same reason, equally good fits can be obtained by making use of SSPs of reasonably different metal content (i.e., solar or half-solar for the intermediate-age and old populations).

Additional constraints that may also be considered, such as the observed ratio between the FIR to V -band and the K - to V -band luminosities, are discussed below.

3.2. The Far-Infrared Emission

All objects have published *IRAS* fluxes at 12, 25, 60, and 100 μm (Devereux 1987), so in principle we might constrain the total light that is absorbed in the model by comparison with the observed total infrared luminosity. By analogy with the observational quantity FIR/ V , defined in the previous section (see Table 1), we compute a theoretical quantity, FIR/ V , representing the ratio between the absorbed light and the quantity $F_i(5550 \text{ \AA})/5550$ (ergs s^{-1}). The absorbed light is easily obtained as the difference between the attenuated and the intrinsic light of the stellar populations that provide the best fit.

However, it is not easy to compare with the corresponding observational quantity, because only a fraction of the radiation emitted in the FIR could be sampled by our slit, whose aperture is smaller than the *IRAS* beam and covers only the central region ($\simeq 1$ kpc) of the galaxy. As discussed in the previous section, aperture problems limit the use of the FIR/ V values. We thus decided to consider the FIR/ V ratio only as an output of the model, to be compared with the values provided in Table 1. It is worth noting that a model that fits the optical data provides only a lower limit to the expected FIR emission (for the assumed extinction law) because of the possible presence of heavily

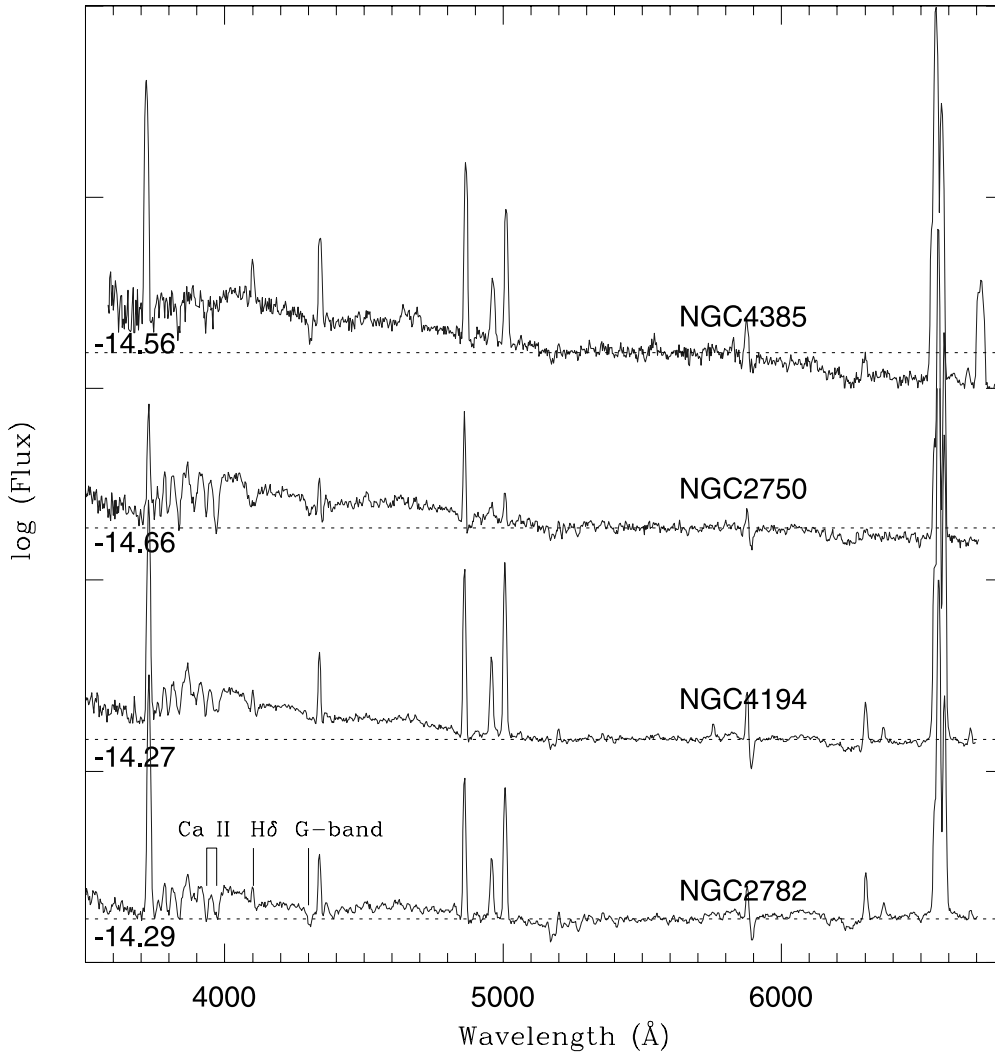


FIG. 1a

FIG. 1.—Observed spectra of the starburst nuclei of our sample galaxies. The spectra are arranged in three panels, with optical colors becoming increasingly redder from NGC 4385 to NGC 4818. The flux scale for each plot is shown by the dotted horizontal line. The value adjacent to this line is the log of the visual flux ($\text{ergs cm}^{-2} \text{s}^{-1} \text{\AA}^{-1}$), and the vertical tick marks are placed at each 0.5 dex. The positions of H δ and the prominent metallic lines are marked. The red part of the spectrum is dominated by the H α emission line, while in the blue part several metallic absorption lines can be seen. Absorption-line strength gradually dominates over the emission-line strength as we move toward higher order Balmer lines, with the H δ line seen only in absorption in the majority of the starbursts. [See the electronic edition of the *Journal* for a color version of this figure.]

attenuated young populations contributing to the FIR but not to the optical emission. For extinction curves that are flatter than the Galactic curve, the model FIR luminosities would be smaller than the values reported in this study.

3.3. The Near-Infrared Emission

For all our program galaxies, Devereux (1989) has provided multiaperture K -photometry at 3".6, 5".3, 7".2, and 9".3 diameters. The origin of the K -band luminosity in nuclear starbursts is one of the key aspects investigated by Devereux. Both the old and intermediate, and even the young populations, can provide a significant contribution to the K -band luminosity. These three populations have observationally distinguishable stellar features in the optical spectrum, especially when one looks at the Balmer discontinuity and the prominence of hydrogen and metallic absorption lines. With our synthesis models we can thus check the consistency of the contribution of the different populations in the NIR and the optical simultaneously.

In order to homogenize the data of Devereux (1989) with ours, we have calculated the fraction of the K -band flux that

falls within our slit aperture. To this purpose, we have computed the surface brightness profile that fits the multiaperture data. The data are consistent with exponential luminosity profiles with scale lengths between 1" and 1".5. This suggests that the source of the K -band luminosity is the stellar disk rather than a very compact source. The maximum luminosity allowed for a compact source is $\approx 50\%$ of that observed within the 3".6 aperture. From the fitted surface brightness profile, we calculated the K -band flux that falls within our slit aperture and then computed the corresponding ratios with the visual flux of our spectra, F_K/F_V . The resulting values are tabulated in column (8) of Table 1.

4. RESULTS AND DISCUSSIONS

The observed spectra of the sample galaxies are shown in Figure 1. These spectra indicate a wide range of optical properties in spite of having nearly similar NIR and FIR luminosities. Spectra are arranged according to their colors in order to easily visualize the gradual change from blue (NGC 4385) to red (NGC 4818) starbursts. The most noticeable

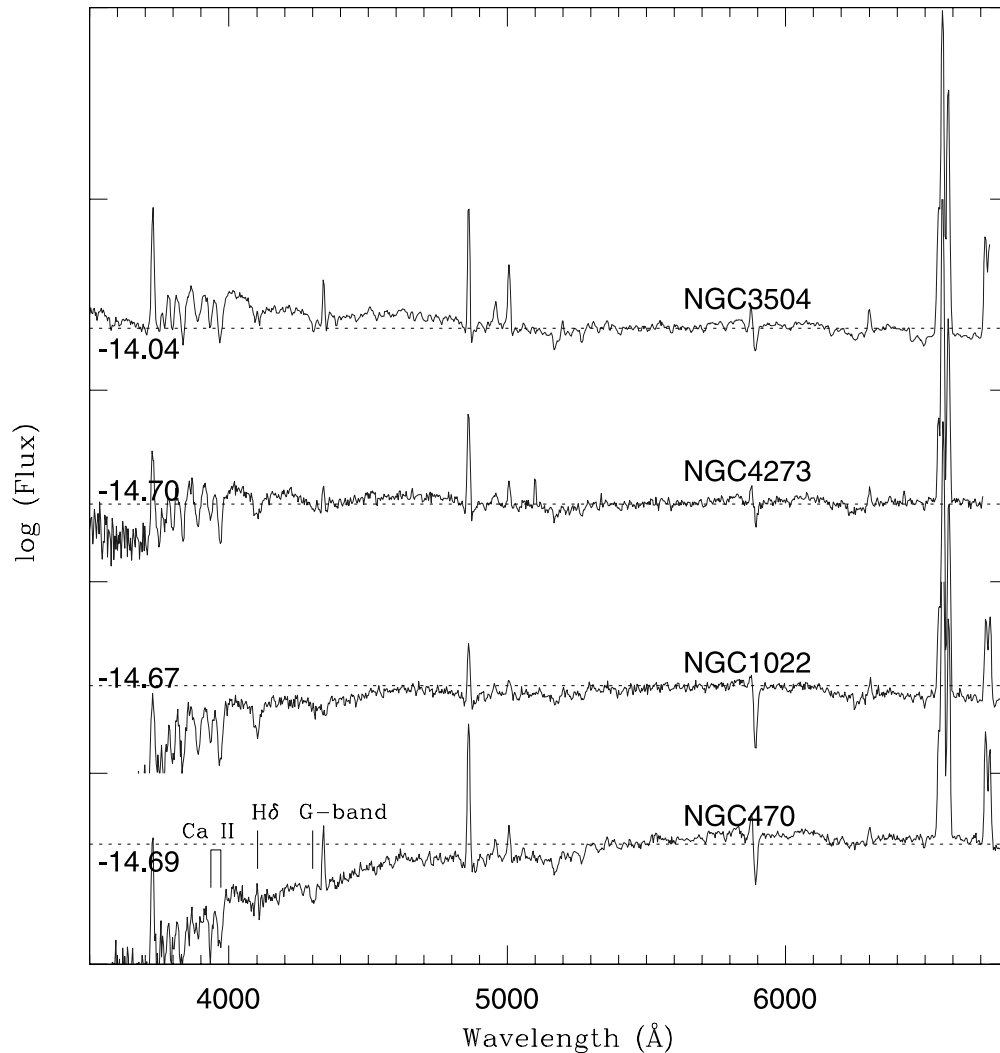


FIG. 1b

characteristic of these spectra is that the $H\alpha$ and $H\beta$ lines are seen in emission, while the higher order lines of the Balmer series are seen in absorption. This characteristic behavior was also present in the sample of very luminous infrared galaxies (VLIRGs) analyzed by Poggianti et al. (2001). The transition from emission to absorption happens at $H\delta$, with 11 of the 12 galaxies having the absorption feature stronger than the emission line. The only exception is the Wolf-Rayet galaxy NGC 4385 (Mrk 52). Besides, several metallic lines, notably the Ca II H and K lines, are also seen in absorption, even in NGC 4385. The simultaneous presence of absorption and emission lines is clearly an indication that more than one population contributes to the observed spectrum.

To disentangle the contribution of the different stellar components, and also to investigate the role of dust in reddening the spectrum, especially in red starbursts, we have applied the model described in the previous section to our starburst spectra. In order to highlight the success of the method, we summarize here the salient characteristics of the different stellar populations. The Balmer emission lines suggest the presence of a young population rich in OB stars. The intermediate-age stellar populations are characterized by the prominence of hydrogen absorption lines and by a strong gradient around 3700 Å. They do not show the discontinuity at

4000 Å (Bruzual A. 1983), which is instead a characteristic feature of the old populations.

Between 3700 and 4000 Å, the spectral shape of the intermediate-age stellar populations is thus very different from that of the old populations. At wavelengths longer than 4000 Å, the continuum of the intermediate-age populations is characterized by the absence of typical absorption bands (e.g., Mg and the G band) shown by the old populations (age > 1 Gyr). Thus, a significant contribution of the old populations not only changes the equivalent width of the hydrogen lines (emission or absorption) but also modifies the shape of the continuum between 3700 and 4000 Å and introduces visible features in the optical region.

Another noticeable characteristic of the old populations is the depth of the Ca II K line at $\lambda \simeq 3934$ Å. This line is almost absent in young and intermediate-age populations. It becomes prominent at ages greater than a few Gyr, and thus it is a strong indicator of the dominance of the old populations. On the contrary, the Ca II H line is blended with the $H\epsilon$ line and may appear strong even for intermediate-age populations. In the present modeling, we have not used the Ca II K line as a constraint because of lack of information on its behavior at different metallicities. Indeed, the atmosphere models used to compute SSPs are based on solar-metallicity stars, and only

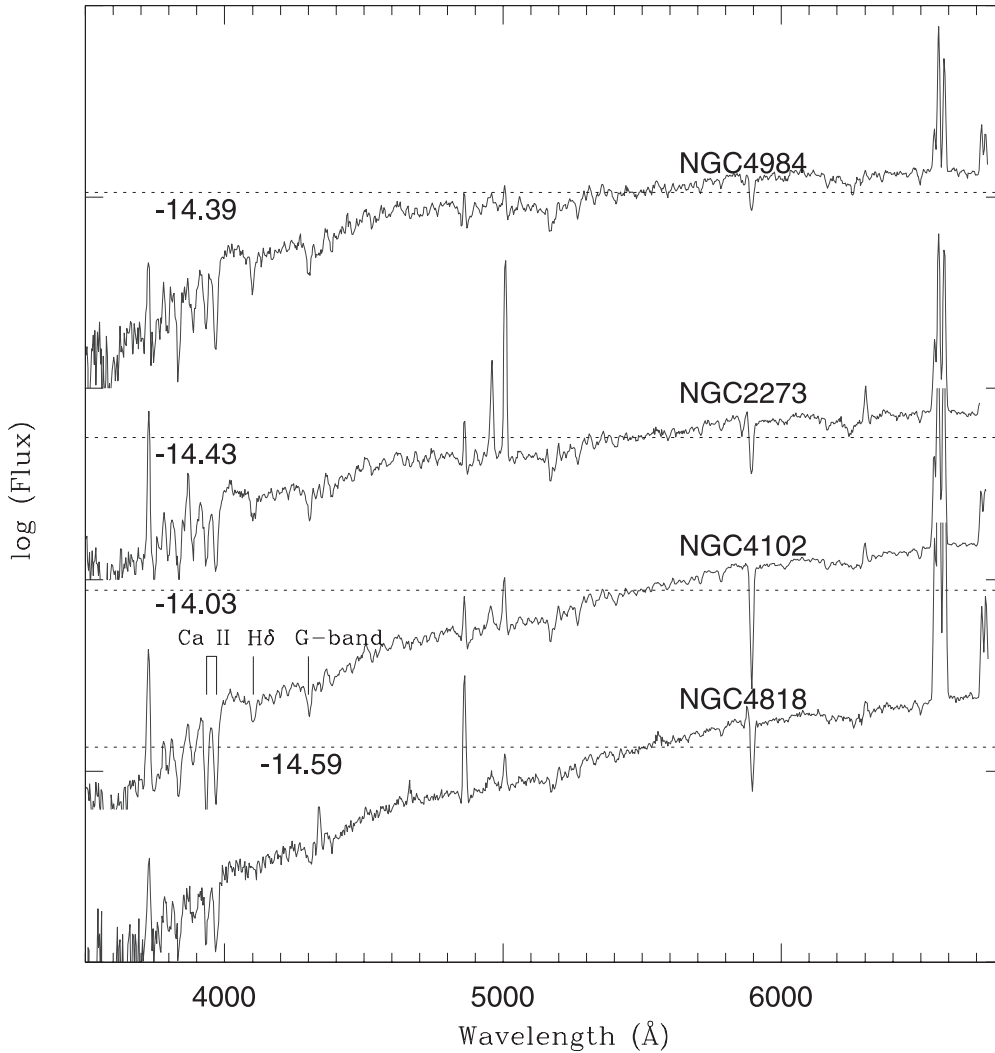


FIG. 1c

the indirect effect of metallicity on the turnoff of the isochrone can be modeled. Recent advances in atmosphere models will allow the inclusion of this constraint in the near future (Rodríguez-Merino et al. 2003). However, although they are not included as a constraint, we may notice that the Ca II K and Ca II H+H ϵ absorption lines are fairly well reproduced by the models, providing a further strong support to the validity of the solution.

In summary, when a good fit to the data is reached, the solution is unique as far as the three broad age ranges are considered. More specifically, while almost equally good solutions can be obtained by interchanging the different populations within a given episode (young, intermediate, or old), it is not possible to find a consistent solution by suppressing or adding an entire episode of star formation.

For the purpose of conciseness, we show in Figure 2 only three model fits, while the results for all the galaxies are presented in Table 2. NGC 4385 and NGC 4984 are selected as representative blue and red starbursts, respectively. NGC 1022 represents an intermediate case. For each galaxy, the bottom panel of the figure shows the best-fit model (lines extending shortward of 3500 Å) superposed on the observed spectrum. The spectra are normalized to their V -band luminosity. The residuals (observed–model) and the estimated errors at the 14

fitted points are shown below the corresponding features. The residuals on the H α , H β , and H δ line bands are identified by circled error bars. The histogram in the top panel represents the star formation history (in $M_{\odot} \text{ yr}^{-1}$) with the relevant SFRs on the left axis. The square at each histogram position represents the color excess $E(B-V)$ for each population. The $E(B-V)$ scale is shown on the right axis.

Models reproduce the observed spectra fairly well, as can be judged by the low residuals at the fitted continuum bands. The fits were even able to reproduce the strength of some of the spectral features, such as the Ca II H and K absorption lines, that were not included in the merit function. The relatively large residuals and errors on H β and H δ lines are due to their small equivalent widths, caused by the stellar absorption lines almost wiping out the nebular emission lines. Observed (Fig. 2, *left column*) and model EWs of H α , H β , and H δ are written on the plots. We did not try to fit the emission lines of [O II] and [O III], because their intensities depend strongly on the physical conditions, in addition to the strength of the stellar populations.

For each starburst, the model has found four populations—two young, one intermediate-age, and one old—each with its distinct mass (or SFR) and extinction. The two young populations may represent either two short-duration bursts, one older than the other, a continuous star formation lasting for

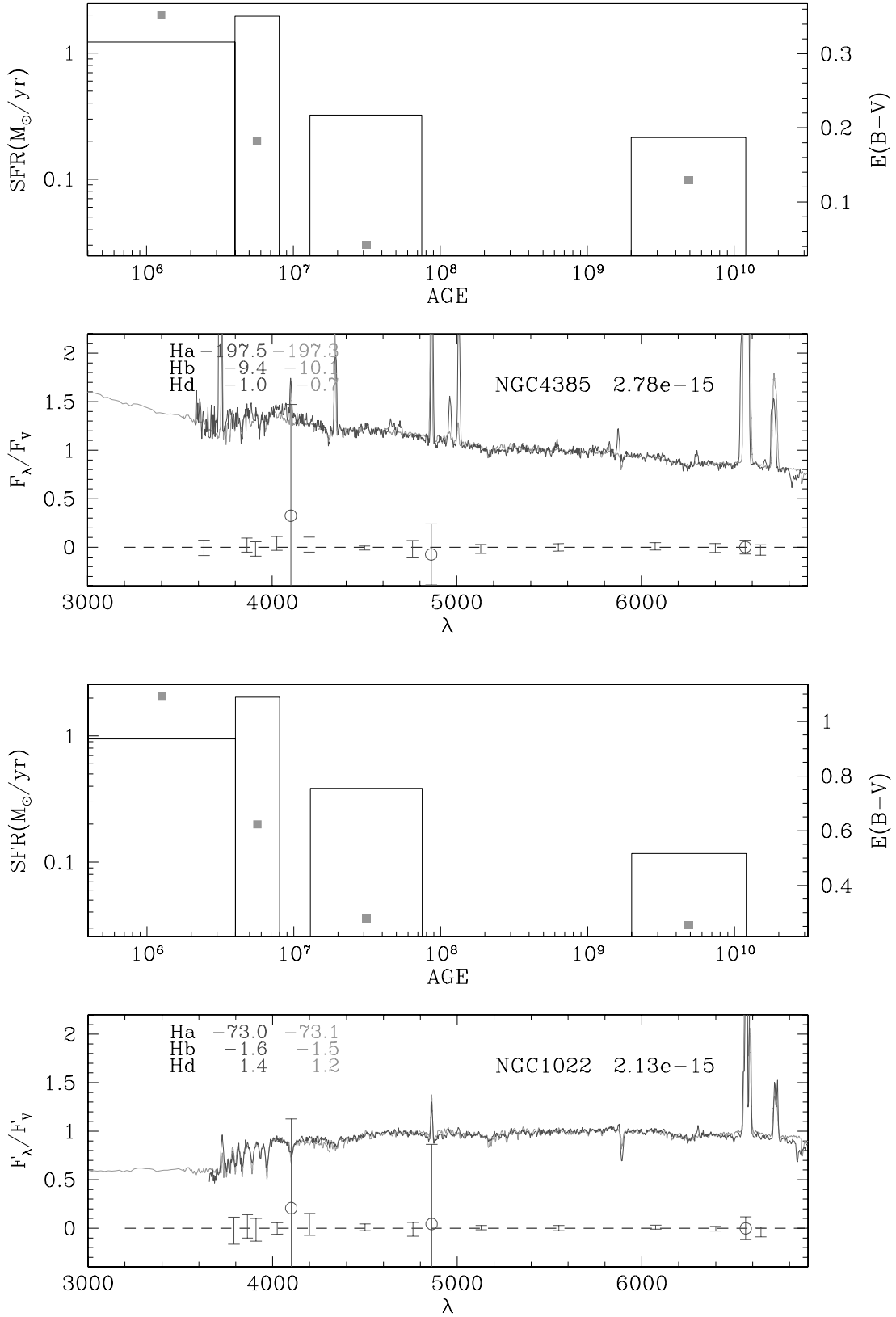


FIG. 2.—Comparison of the observed nuclear spectra of three representative program galaxies with the model spectra (*bottom plot in each panel*). The residuals (observed—model) at each of the fitted bands are shown below the spectrum, along with the error bars, with the circled error bars corresponding to the residuals at the line bands. The inferred star formation history is shown by the histograms in the upper panel. The squares correspond to the color excess $E(B-V)$ (numbers on the right axis) for each star formation episode. Fits for NGC 4385, NGC 1022, and NGC 4984 are shown. These three galaxies represent blue, intermediate-color, and red starbursts, respectively. [See the electronic edition of the Journal for a color version of this figure.]

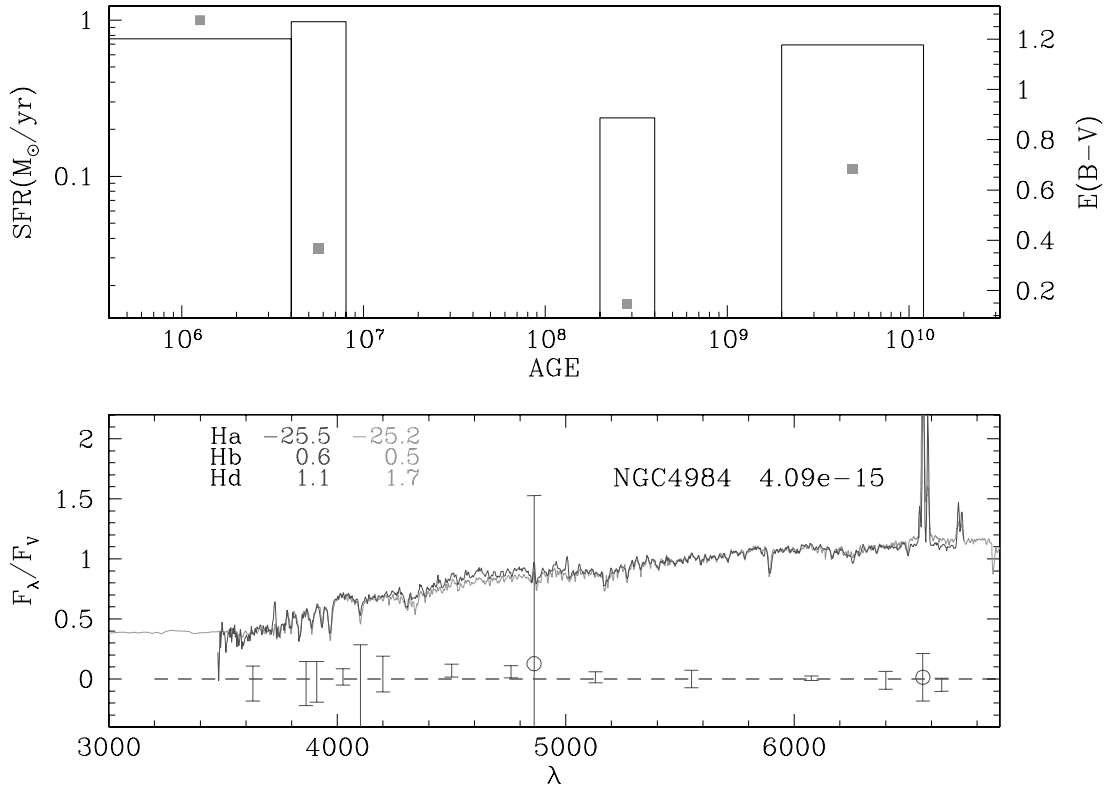


FIG. 2.—Continued

more than 4 Myr, or two bursts of nearly the same age but with vastly differing extinction.

The results of the fit for all the galaxies are presented in Table 2. Columns (2)–(10) contain the model-derived SFR and the reddening $E(B-V)$ for the four selected populations. For the intermediate-age population, we also tabulate the age of the best-fit SSP in column (8). Model derived ratios FIR/V and F_K/F_V are given in columns (11) and (12), respectively. The last column contains the total mass sampled by the slit with the adopted IMF.

A comparison of the computed FIR/V values and the observed values (cols. [6] and [7] of Table 1) indicates that the two are in the same range, taking into account the differences in the optical and FIR apertures discussed in § 3.2. It may be recalled that in VLIRGs, which on average are 10 times more luminous than our galaxies, observed values are systematically higher than the model values, suggesting a significant amount of star formation hidden from the optical view (Poggianti et al. 2001). The fact that the observed values are comparable with the predictions of the model in our sample of galaxies implies that

TABLE 2
STAR FORMATION AND REDDENING PROPERTIES OF THE STARBURST NUCLEI

NGC (1)	YOUNG BURST				INTERMEDIATE			OLD (BULGE OR DISK)		FIR/V MODEL (11)	F_K/F_V MODEL (12)	MASS ($10^9 M_\odot$) (13)
	(0–4 Myr)		(4–8 Myr)		Age							
	SFR (2)	$E(B-V)$ (3)	SFR (4)	$E(B-V)$ (5)	SFR (6)	$E(B-V)$ (7)	Age (Myr) (8)	SFR (9)	$E(B-V)$ (10)			
470.....	1.78	0.73	4.46	0.66	1.91	0.49	300	0.39	0.40	21.88	0.37	4.35
1022.....	0.95	1.09	2.04	0.62	0.39	0.28	50	0.12	0.25	27.83	0.33	1.21
2273.....	3.77	1.28	0.15	0.00	0.34	0.00	50	1.62	0.55	22.86	0.45	16.26
2750.....	2.95	0.98	1.90	0.00	0.35	0.00	50	0.52	0.33	17.00	0.23	5.25
2782.....	4.26	0.65	3.48	0.00	0.52	0.00	50	2.07	0.51	12.49	0.32	20.73
3504.....	8.24	1.14	2.62	0.00	0.30	0.00	100	1.06	0.44	34.08	0.29	10.65
4102.....	7.25	1.78	0.00	2.53	0.10	0.00	50	1.01	0.66	100.18	0.70	10.10
4194.....	18.32	1.05	5.49	0.00	0.45	0.00	300	1.51	0.53	47.42	0.29	15.34
4273.....	0.58	0.92	0.19	0.00	0.09	0.00	50	0.18	0.41	15.90	0.28	1.79
4385.....	1.22	0.35	1.95	0.18	0.32	0.04	50	0.21	0.13	9.86	0.16	2.16
4818.....	5.08	1.59	0.08	0.00	0.02	0.00	300	0.43	0.68	154.38	0.72	4.34
4984.....	0.77	1.27	0.99	0.37	0.24	0.15	300	0.70	0.68	18.25	0.57	7.09

most of the FIR emission detected by *IRAS* originates in the starburst nucleus and that the starburst regions do not contain a significant amount of optically hidden star-forming regions.

An insight into the relative importance of the young, intermediate-age, and old populations in the overall history of nuclear star formation can be obtained by analyzing the spectra of individual populations. In Figure 3, we plot the best-fit model spectrum, along with the spectra of individual populations for the three representative galaxies. Observed *K*-band photometry is also displayed in these plots. Note that the plotted spectra are attenuated by the extinction values obtained for each population.

In the following subsections, we discuss in detail the mass and extinction of the different populations.

4.1. Masses of the Distinct Populations

In the presence of selective extinction, deriving masses of different populations is not straightforward. While the intrinsic mass-to-light ratio is the basic ingredient of any population synthesis technique, the option to vary attenuation for each

population introduces a new degree of freedom. Unreasonably high masses can be obtained by letting the attenuation increase with the strength of an intermediate or old stellar population. The algorithm described in § 3 automatically copes with this degeneracy by selecting the minimum mass-to-light ratio solution.

Mass, rather than SFR, is the fundamental output of the model. The SFR of each population, tabulated in Table 2, is obtained by dividing the mass by the assumed duration of star formation (see § 3.1). The derived mass of each population is plotted as a bar histogram in Figure 4. For each galaxy, the histograms from left to right denote the masses of young, intermediate-age, and old populations. It can be seen that the mass of the young population is comparable to that of the intermediate-age population in most cases, whereas the mass of the old population is significantly higher. The mass of the young population is plotted against the old stellar mass in Figure 5. The dotted lines in this plot delimit the zone in which the young stellar mass is 0.1% and 1% of the old stellar mass. All the points lie between these two limits. This

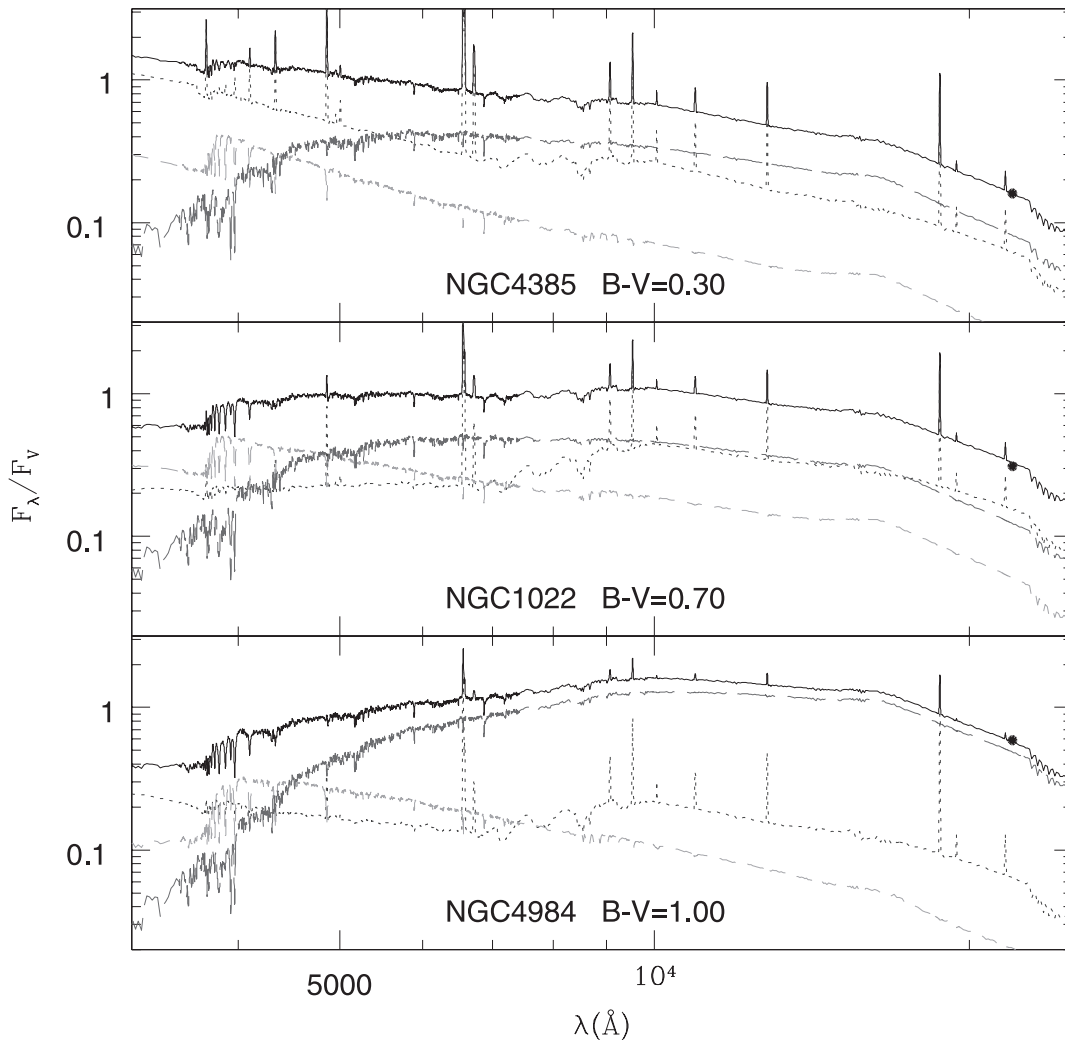


FIG. 3.—Decomposition of the best-fit model spectrum (*solid line*) into spectra of young (*dotted line*), intermediate-age (*short-dashed line*), and old (*long-dashed line*) populations, for three representative sample galaxies. NGC 4385 is the bluest of the sample galaxies, while NGC 4984 is among the reddest of the sample galaxies. The thick dot at the $2.2 \mu\text{m}$ represents the estimated *K*-band flux (normalized to the *V* flux) within the spectroscopic slit. The blue part of the spectrum is dominated by the young and intermediate populations, while the red and NIR parts are dominated by the old population. [See the electronic edition of the *Journal* for a color version of this figure.]

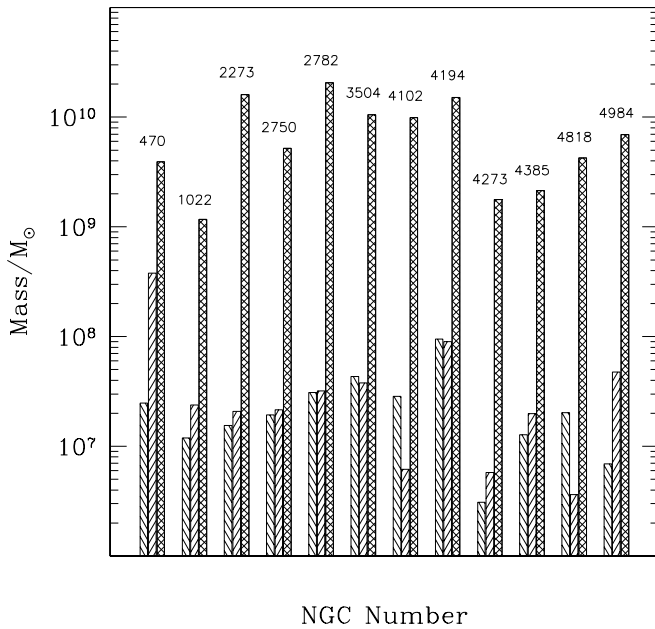


FIG. 4.—Masses of the young (left vertical bar), intermediate-age (center vertical bar), and old (right vertical bar) component, sampled by our slit. While the first two masses are within a factor of 2 of each other in most cases, the old-population mass is up by as much as a factor of 100.

indicates that the recent starburst contributes a tiny amount to the overall visible mass of the nucleus. It is interesting to note that the corresponding fraction is 5% in blue compact galaxies (Pérez-González et al. 2003). The inferred total stellar masses of the starburst regions are in the range of masses that are usually derived for the galactic bulges.

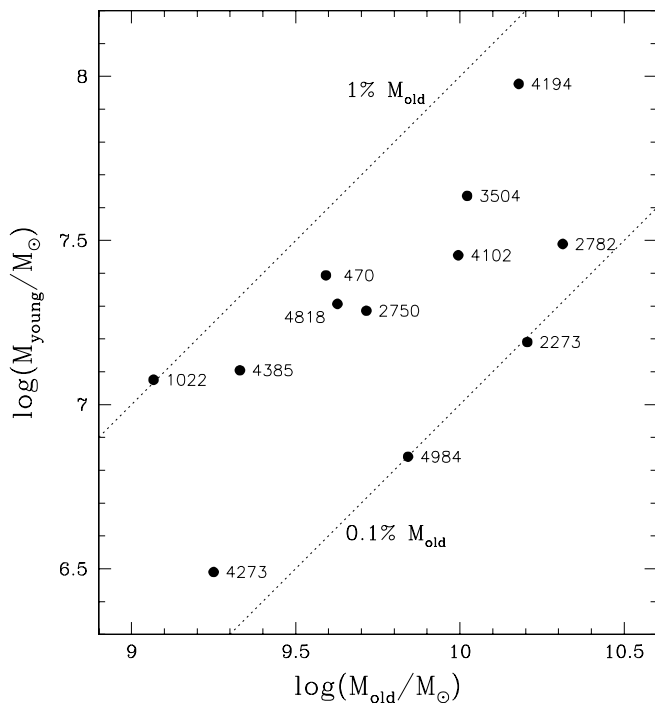


FIG. 5.—Mass of the young component (proportional to the current SFR) vs. mass of the old component. Dotted lines correspond to the boundaries where the young burst mass is 0.1% and 1% of the total mass. The observed trend implies that the young mass is proportional to the old mass.

4.1.1. Present versus Past Star Formation in Starburst Nuclei

The ratio between the current star formation rate (in the last 8 Myr) and the average past star formation rate, $\text{SFR}/(\text{SFR})$, often referred to as the birthrate parameter (Kennicutt, Tamblyn, & Congdon 1994), is useful for measuring the strength of the most recent burst. The value of this ratio is less than 0.1 for normal early-type disk galaxies, which are the Hubble types that dominate our sample. Our sample of starbursts have a birthrate parameter in the range 1–12, with an average value of $\approx 5.0 \pm 3.3$. This reiterates that the galaxies of our sample are indeed starburst galaxies.

All starburst regions are found to have an intermediate-age stellar population. Unfortunately, it is difficult to distinguish differences in spectral features of an evolving starburst between ~ 15 and 500 Myr. An evolved spectra of an intense short-duration burst will be indistinguishable from that of a lower intensity continuous star formation process. There can be three possible origins for the intermediate-age population: (1) it represents stars formed earlier in the current star formation episode, (2) it represents the exponential tail of the disk star formation history, or (3) it represents an episode of star formation similar to the present one but that took place around a few hundred million years ago. In the following paragraphs we discuss these possibilities in more detail.

In the majority of our sample galaxies, the best-fit SSP that represents the intermediate-age population has an age of 50 Myr (see col. [8] in Table 2). Considering that the SED remains almost unchanged between 15 and 75 Myr, the intermediate-age population could be as young as 15 Myr. Case 1 would then imply that the star formation has been going on uninterrupted for at least 15 Myr. The histograms of Figure 2 suggests that there is a gap in star formation between 8 and 15 Myr. This gap corresponds to the populations of red supergiants, which are also represented by the 7 Myr SSP. Hence, equally good solutions could have been obtained by extending the duration of the young burst up to 15 Myr. The average present SFRs, in that case, would be a factor of 2 lower than those presented in Table 2. If the SFR remains constant, then the mass of the processed stars scales proportionately with the duration of the burst. We have seen in the previous section that the mass of the intermediate-age population is comparable to that of the young population. This implies that the duration of the intermediate-age population is comparable to that of the young population (~ 15 Myr). The duration would be even smaller if the SFRs were higher at earlier times. Hence, the maximum duration of the present episode for a continuous star formation model is ~ 30 Myr.

If case 2 above is correct, then the masses of the populations would be proportional to the lifetime of the stars constituting the populations. This would imply that the mass of the intermediate-age population is around 1% of that of the old population. The SFR in the disks of early-type galaxies decreases exponentially with time, and the expected mass would be even less. The derived masses of the intermediate-age populations are indeed $\leq 1\%$ of that of the old population, and hence we cannot rule out case 2. The third possibility, case 3, is also plausible because the mass of the intermediate-age population is comparable with that of the present burst.

Perhaps a way to distinguish case 2 from the other two cases is to look at the spatial distributions of the stellar populations. In case 2, stellar populations are expected to be uniformly distributed, whereas in cases 1 and 3 old star clusters are expected. The fact that SSCs are frequently encountered in

starburst regions and that some of them are of intermediate age and spatially separated from the present active knot makes us believe that case 3 is the most likely possibility. It is also possible that all three processes of formation of intermediate-age population are at work in starburst regions. The relative importance of the three processes might vary from one galaxy to another.

4.2. The Origin of K -Band Luminosity

The origin of the K -band luminosity in nuclear starbursts has been the subject of debate ever since the first starburst sample was defined by Balzano (1983). She found that the NIR colors, as well as the K -band luminosities, were unaffected by the starburst activity. This can be seen in Table 3, in which we have tabulated Balzano's $H-K$ and $J-K$ colors of starburst and bright NGC galaxies in columns (2) and (3), respectively. NIR colors of starburst nuclei are indistinguishable from those of the nuclei of normal galaxies. Cizdziel, Wynn-Williams, & Becklin (1985) supported Balzano's findings by analyzing the K -band growth curves of starburst nuclei, which indicated a lack of central concentration. On the other hand, Rieke et al. (1980, 1993) interpreted the entire K -band luminosity in the archetype starburst M82 as due to the red supergiants associated with the present starburst activity.

Our sample of starburst galaxies is well suited to resolve the above controversy. Devereux (1989), from which our sample was chosen, discussed the existence of a correlation between the K band and the $10\ \mu\text{m}$ luminosities for galaxies that are luminous at $10\ \mu\text{m}$. Since $10\ \mu\text{m}$ emission is related to recent star formation, this correlation implies that the K -band emission is also related to the recent star formation. On the contrary, by means of our detailed population synthesis technique, we find that in the same galaxies showing the correlation between $10\ \mu\text{m}$ and K -band luminosity, a major fraction of the K -band emission comes from the old population. A strong contribution to the K -band luminosity from the young and/or intermediate-age stellar populations is excluded by the overall fit of the broad continuum features and inspection of some metallic lines (e.g., Ca II K) of the optical spectrum. To better clarify this point, we plot in Figure 6 the fractional contribution of the old stars to the total K -band luminosity against the birthrate parameter. We also show a comparison with theoretical predictions based on the SSP, assuming that the old stars have an average age of 10 Gyr. Calculations were done for two ages of the young component: 10 and 5 Myr, which represent phases of starburst with and without the red supergiants, respectively. The metallicities for the young and old components were assumed to be the same. The age of the young component and the metallicities for the different plotted lines are (1) 10 Myr and $Z = 2.5 Z_{\odot}$ (solid line), (2) 10 Myr and $Z = Z_{\odot}/5$ (dotted line), (3) 5 Myr and $Z = 2.5 Z_{\odot}$ (short-dashed line), and (4) 5 Myr and $Z = Z_{\odot}/5$ (long-dashed line), respectively.

As expected, the contribution of the old population decreases with increasing birthrate, but only for a birthrate

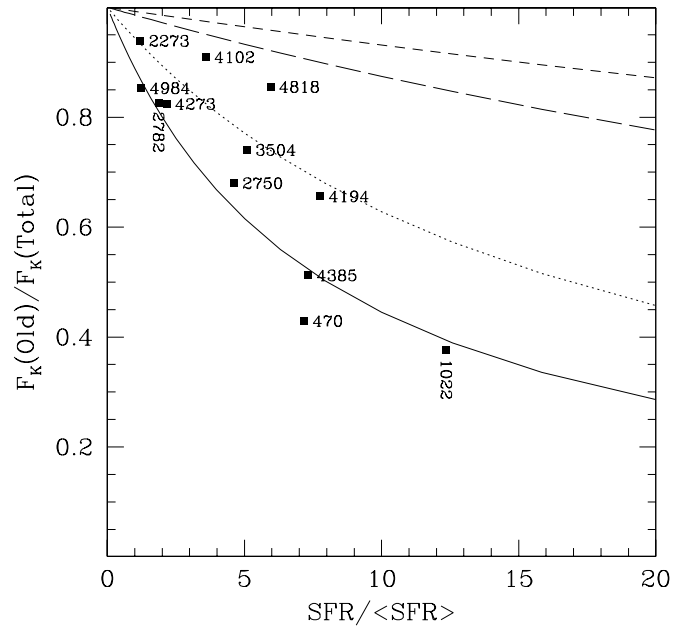


FIG. 6.—Fractional contribution of the old stars to the K -band luminosity vs. the birthrate parameter. As expected, the contribution of the old stars to the K band decreases with increasing birthrate. In three-quarters of the sample galaxies, the fraction remains above 60%. Lines represent theoretical predictions using SSPs and refer to the following: $Z = 2.5 Z_{\odot}$, young age 10 Myr, and old age 10 Gyr (solid line); $Z = Z_{\odot}/5$, young age 10 Myr, and old age 10 Gyr (dotted line); $Z = 2.5 Z_{\odot}$, young 5 Myr, and old 10 Gyr (short-dashed line); $Z = Z_{\odot}/5$, young 5 Myr, and old 10 Gyr (long-dashed line).

parameter larger than about 7 does this contribution fall below 50% of the total light. We have only two cases in which this contribution is less than 50%: NGC 470 (42%) and NGC 1022 (38%). NGC 1022 is among the galaxies with the lowest SFRs in our sample ($1 M_{\odot} \text{ yr}^{-1}$), and its high birthrate is due to the low mass of the old population. This is to stress once more that the relative contributions of the young and the old populations to the K band depend on the birthrate parameter rather than the present SFR. The figure also illustrates the dependence of the contribution of the old population on the age of the dominant young population and the metallicity. For a given birthrate, the contribution of the old population is higher for lower age and lower metallicity of the young population. It can be inferred from the theoretical curves in the plot that for young bursts that are yet to evolve into the red supergiant phase, more than 80% of the K -band flux originates from old stars, unless the birthrate parameter is much higher than the plotted range.

Note that a lower contribution from the old population in NGC 1022 may also be inferred from the relatively low strength of the Ca II K line (Fig. 1).

Further insight about the nature of the K -band emission may be obtained by analyzing the radial intensity profiles. As discussed in § 3.3, the Devereux (1989) multiaperture

TABLE 3
NIR COLORS OF NUCLEAR STARBURSTS AND NORMAL GALAXIES

Color (1)	Balzano (2)	Bright NGC (3)	M82-like (4)	Young Burst (5)
$H-K$	0.32 ± 0.12	0.31 ± 0.10	0.34 ± 0.05	0.51 ± 0.17
$J-K$	1.02 ± 0.12	1.04 ± 0.10	1.08 ± 0.08	1.05 ± 0.14

K -photometry is consistent with exponential luminosity profiles (scale lengths between $1''$ and $1''.5$), with the compact nucleus not contributing more than 50% within the $3''.6$ aperture. The contribution of the compact nucleus would be even less if the real intensity profiles of program galaxies were $r^{1/4}$ bulge profiles rather than the exponential ones that we have assumed. This disagrees with the Devereux claim of “central concentration” of K -band flux in these galaxies. We, however, find evidence of systematic reddening of $V-K$ color toward the center, which is expected in all disk galaxies because of the flattening of the disk at shorter wavelengths due to optical depth effects in *dusty* disks (Burstein, Haynes, & Faber 1991; Evans 1994).

In light of this new analysis, we may ask what is the origin of the correlation found between the K -band and $10\ \mu\text{m}$ luminosity in these galaxies. Figure 5 helps us to clarify this point. In this figure, the mass of the young component, which is directly proportional to the SFR, is compared with the mass of the old component, essentially the total mass of the bulge. There is a trend for the more massive galaxies to host a stronger nuclear starburst.

Thus, the relation between the K -band and $10\ \mu\text{m}$ luminosity can essentially be ascribed to the underlying relation between the total galaxy mass (hence, the mass of the old component and the K -band luminosity) and the gas mass (hence, the SFR and $10\ \mu\text{m}$ luminosity).

This explanation is also supported by the fact that Devereux’s M82-like starburst sample galaxies are earlier than Sb (and hence relatively bigger), while the mean Hubble type of Balzano’s sample is Sc. On the other hand, the observed lack of high $10\ \mu\text{m}$ emission in faint K -band sources is basically due to the lower gas mass (not fraction) of low-mass galaxies. Thus, the M82-like starburst sample of Devereux contains early type star-forming galaxies.

Interestingly, the $J-K$ and $H-K$ colors of the models that best fit the observed spectra agree excellently with those reported for Balzano’s sample of starburst galaxies (Balzano 1983). This is demonstrated in Table 3. Model colors of the total and only the young burst are given in columns (4) and (5), respectively. It can be seen that the observed $H-K$ colors of starburst galaxies are indistinguishable from those of non-star-forming NGC galaxies.

Thus, most of the K -band luminosity of our starburst nuclei seems to originate from old disk/bulge stars. However, we expect that in starbursts with a birthrate parameter that exceeds the average value found in our sample (about 5), the young stars begin to dominate the NIR fluxes. This may be the case of high-redshift starbursts with similar SFRs but with a significantly lower number of old stars.

4.3. Extinction Pattern of Different Stellar Populations

One of the aspects in which our approach to spectral decomposition differs from the rest (e.g., Lançon et al. 2001) is in the treatment of extinction. In our starburst models, the extinction of each population is a free parameter, whose value is chosen to be consistent with both the continuum shape and the Balmer line ratios. In addition, the derived extinction does not depend on the extent of contamination by the underlying absorption, as the old populations are simultaneously determined in the models.

The dots above the histograms in Figure 2 indicate the reddening value of each population. The reddening values, $E(B-V)$, of each population are also given in Table 2. It can be

seen that the reddening of the young populations (age of ≤ 8 Myr) is always higher than that of intermediate-age and old populations. Poggianti et al. (2001) also found a similar result for a sample of VLIRGs. The reason for the higher extinction of the young population is well known—the young population is still embedded in its parent molecular clouds, which are known to be dusty (Silva et al. 1998). Among the two young populations, the extinction of the youngest population is systematically higher. This may suggest that stars are already escaping from their parent molecular clouds at around 4 Myr.

The ratio of the extinctions of the old and young populations is plotted against the extinction of the young population in Figure 7. The latter value is calculated from the summed model spectra of the two youngest populations (see the description of Table 1 in § 2 for more details). The dotted line in the figure represents the average value of the ratio for the sample galaxies, which is equal to 0.43 ± 0.13 . Note that the rms of the ratio is only 0.13 mag, in spite of a range of more than 4 mag for the extinction of the young population. Thus, the observed extinction toward the old stars is proportional to the extinction toward the young stars. Such a correlation is not expected if all the dust that causes the extinction of the old stars is mixed with the stars. Moreover, the $E(B-V)$ of the old population in all cases, except NGC 4385, is higher than 0.18 mag, the limiting reddening for a uniform mixture of dust and stars (Poggianti et al. 2001). All these arguments suggest that the same clouds that cause the extinction of the young population are the principal contributors to the extinction of the old stars. This could be understood under a geometry in which the young star-forming regions are surrounded by molecular clouds and the majority of the old (bulge/disk) stars are distributed uniformly around these clouds. Only the light from the old stars that are behind the cloud would suffer high extinction, whereas the light

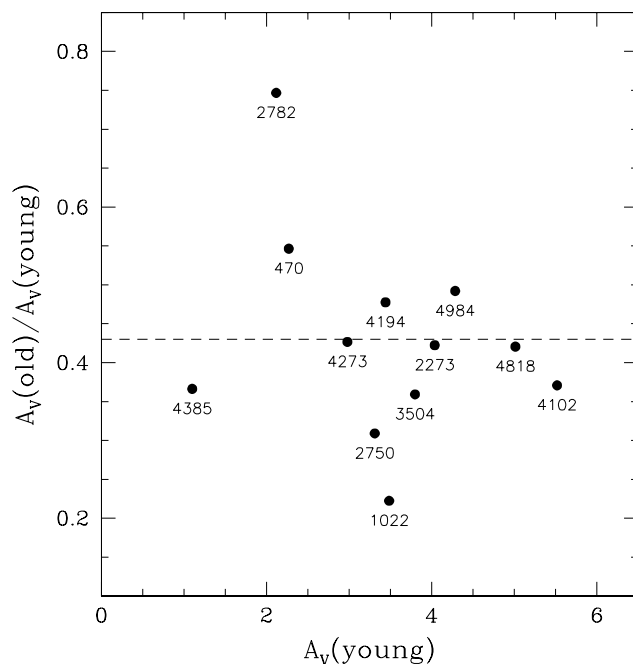


FIG. 7.—Ratio of the visual extinctions of the old and young population, vs. the visual extinction of the young population. The dotted line shows the mean value of the ratio. Note that the mean ratio is essentially the same as that obtained by Calzetti et al. (1994).

from the rest of the stars would have a maximum reddening of $E(B - V) = 0.18$ mag. The net extinction of the old population happens to be 43% of that of the young population. Galaxies with a ratio considerably lower than the mean ratio (e.g., NGC 1022) may be those in which the young star-forming region is located at the far side of the bulge/disk, and vice versa.

Analyzing a sample of starburst nuclei, Calzetti et al. (1994) noticed that the continuum near $H\alpha$ and $H\beta$ suffered about half the attenuation suffered by the nebular lines. Our result would be identical to that obtained by Calzetti et al. if the near-ultraviolet and optical continua are predominantly contributed by the old stars, i.e., stars that do not supply ionizing photons. We have demonstrated that this is indeed the case in previous subsections. Hence, our detailed analysis reinforces the interpretation put forward by Calzetti et al. (1994), that the reason for a lower extinction for the continuum than for the emission lines is the relatively lower extinction toward the older stars than the young massive stars. Our analysis also suggests, for instance, that the extinction ratio determined from the optical spectrum cannot be simply extrapolated to the ultraviolet because of the different contributions of the old and young populations at these wavelengths (see, e.g., Panuzzo et al. 2003, for a thorough discussion of this problem).

In most cases, we find the reddening of the intermediate-age population to be lower than that of the old population. Is it a real effect, or is it due to some inherent limitation of the model used? In order to address this question, we go back to Figure 3, where the typical contributions of the three populations are plotted. It can be seen that the wavelength range in which the intermediate-age population contributes, if at all, covers less than 500 Å—between the blue limit (~ 3600 Å) and $H\delta$. In this range, there are only two galaxies (NGC 470 and NGC 1022) in which the intermediate-age population is the dominant contributor. Significantly, the derived extinctions of the intermediate and old populations compare well in these two cases. In the rest of the galaxies, the available baseline is too small to reliably estimate the reddening. The size of intermediate-age population in most galaxies is basically determined from the observed strength of the $H\delta$ line. As our criterion was to choose models that have minimum extinction (or equivalently, minimum mass-to-light ratio), the models are able to give only a lower limit to the extinction of the intermediate-age population. A fair estimate of the mass of the intermediate-age population may be obtained by assuming that it has the same reddening as that of the old population. We find that this mostly affects those cases in which the mass of the intermediate-age population is significantly less than that of the young population. In such cases, the masses estimated this way turn out to be almost equal to those of the young population. In the rest of the cases, the masses increase by around 40%.

4.4. Effect of Older Populations on the Balmer Equivalent Widths

The flux ratios and equivalent widths of Balmer emission lines are often used as diagnostics of extinction and age of the most recent burst in starburst regions. The existence of previous generations of stars, if not taken into account, can seriously affect the determination of both the extinction and age of the young burst. Older populations have two effects: (1) the intermediate-age populations have strong Balmer absorption lines in their spectra, which can decrease the flux

of the emission lines, and (2) the old population can contribute significantly to the continuum, which can lower the emission equivalent width. The latter effect is often referred to as dilution. For an accurate determination of the extinction value, it is necessary to correct for the contamination from underlying stellar absorption lines, and for the age determination it is necessary to know the dilution factor, f_{dil} , which is the ratio of the observed continuum flux to that of the young burst. The following equations are used to calculate the true emission line flux, $f(\text{line})$ and equivalent width, $EW_{\text{young}}(\text{line})$, from the observed equivalent width, $EW_{\text{obs}}(\text{line})$, and continuum flux, $f_{\text{tot}}(\text{cont})$:

$$f(\text{line}) = [|EW_{\text{obs}}(\text{line})| + \Delta EW(\text{line})]f_{\text{tot}}(\text{cont}), \quad (2)$$

$$EW_{\text{young}}(\text{line}) = [|EW_{\text{obs}}(\text{line})| + \Delta EW(\text{line})]f_{\text{dil}}, \quad (3)$$

where $\Delta EW(\text{line})$ is the correction term, which McCall et al. (1985) found to be 2 Å for the prominent Balmer lines. McCall et al. determined this value empirically for a large number of $H\text{ II}$ regions, by forcing the extinction-corrected ratios of the first three Balmer lines to their photoionization values. On the other hand, Veilleux et al. (1995) measured the absorption EWs of $H\beta$ using simultaneous fitting of the emission and absorption lines for a large sample of infrared luminous galaxies. The measured values ranged from 1 to 3 Å, with a median value of 2 Å.

The decomposition of the observed spectra into the spectra of individual populations allows us to make an independent determination of $\Delta EW(\text{line})$; $\Delta EW(\text{line})$ depends on the equivalent width and the relative continuum contribution of intermediate-age and old populations. We summed up the spectra of intermediate-age and old stellar populations to get a pure absorption line-dominated spectrum for each of our starburst nuclei. We then measured the EW and continuum fluxes for the first four lines of the Balmer series in both the total and absorption-line-dominated spectrum; $\Delta EW(\text{line})$ and the dilution factor f_{dil} are then simply given by

$$\Delta EW(\text{line}) = EW_{\text{old}}(\text{line}) \frac{f_{\text{old}}(\text{cont})}{f_{\text{tot}}(\text{cont})} \quad (4)$$

and

$$f_{\text{dil}} = \frac{f_{\text{tot}}(\text{cont})}{1 - f_{\text{old}}(\text{cont})}, \quad (5)$$

where $EW_{\text{old}}(\text{line})$, and $f_{\text{old}}(\text{cont})$ are the equivalent width and continuum flux of the old population alone.

Table 4 contains the statistical properties of $\Delta EW(\text{line})$ and f_{dil} for the four Balmer lines. The mean underlying absorption correction to $H\alpha$ is 1.6 ± 0.3 Å, whereas for the other three lines it is close to 2.4 ± 0.8 Å. The errors on the EWs are the rms deviations for the sample and not errors in the measurements. Hence, the difference in the mean values for $H\alpha$ and the rest of the lines is significant, although the average values are within the quoted errors. On the other hand, it is the practice to use a correction of 2 Å for all the lines, following McCall et al. (1985). It may be recalled that McCall et al. had forced the correction to be the same for all the Balmer lines. In this work, we show that this assumption is not strictly true and that the average value of 1.9 ± 0.3 Å obtained by McCall et al. is a compromise value for all the lines. We emphasize that in a given

TABLE 4
CORRECTION TO EWs AND DILUTION FACTORS

Parameter	$\Delta\text{EW}(\text{line}) \text{ \AA}$				$f_{\text{dil}} = \frac{f_{\text{H}\alpha}(\text{cont})}{1 - f_{\text{H}\alpha}(\text{cont})}$			
	H α	H β	H γ	H δ	H α	H β	H γ	H δ
Average	1.57	2.48	2.32	2.49	4.7	3.2	2.7	2.4
rms.....	0.26	0.60	0.74	0.91	1.9	1.2	0.9	0.8
Min.....	1.15	1.48	1.20	1.22	2.3	1.6	1.4	1.3
Max.....	2.11	3.33	3.28	3.81	22.5	31.3	40.2	46.2

galaxy, the correction to H α is always smaller than that for the other three lines. The average value of the correction could be sample-dependent. This is because the exact numerical value of the correction depends on the relative contribution of the intermediate-age population, which could be different in different star-forming regions. For instance, Kennicutt (1992) found a mean value as high as 5 \AA for the integrated spectra of galaxies. We believe that the average values obtained by us are representative of starburst nuclei of nearby galaxies, and hence we recommend the use of these values for a reliable estimation of A_V and metallicity from nebular lines in starburst nuclei.

The mean dilution factors of the H α and H β EWs are 4.7 ± 1.9 and 3.2 ± 1.2 , respectively, for our sample of starburst nuclei. Observed EWs of starburst nuclei are generally lower than those expected for young bursts (e.g., Veilleux et al. 1995). The analysis carried out in our work supports the idea that an underlying old population is the primary cause for the observed low values of the Balmer EWs in starburst nuclei.

5. SUMMARY AND CONCLUSIONS

We have analyzed optical spectra of a sample of starburst galaxies that have far-infrared, 10 μm , and K -band luminosities similar to those of the prototype starburst M82. We have adopted a theoretical approach that allows us to resolve their star formation history into three major episodes, the ongoing star formation (< 8 Myr), the intermediate-age population (50–500 Myr), and the old populations (older than 1 Gyr).

The extinction of these three main populations is a free parameter and is fixed, together with the star formation history, by the simultaneous fitting of the EWs of the main hydrogen lines and a number of narrow bands in the continuum. These data are complemented by the K -band flux, estimated for the area within our slit from existing aperture photometry. The FIR emission could also be used to constrain the model, but its uncertain contribution within our slit prevented us from using it as a firm constraint.

All galaxies have clear signatures of the above three main episodes of star formation, with birthrate parameter (current SFR over average past value) between 1 and 12. The mass of the intermediate population is generally comparable to the mass formed during the current burst, and together they provide only a small contribution to the total mass sampled by our spectra. The spectra sample approximately the central 1 kpc region, and the mass within this region turns out to be between 10^9 and $2 \times 10^{10} M_{\odot}$, with an average value of $\simeq 8 \times 10^9 M_{\odot}$. These values are within the mass range found for bulges of spiral galaxies. There is a clear tendency for the most massive bulges to host a stronger starburst activity. The mass of the young component increases linearly with that of the old bulge: $M_{\text{young}} \simeq 0.003 M_{\text{old}}$.

The relation between the masses of the young and old components is the most likely cause of the correlation reported by Devereux (1989) between the 10 μm luminosity, which is proportional to the present SFR (i.e., the mass of the young component), and the K -band luminosity, which is proportional to the old component. This correlation led Devereux to conclude that the K -band luminosity is mainly produced by red supergiant stars of the young component. On the contrary, our population synthesis technique allows us to exclude this possibility. In the majority of the cases, the old population contributes more than 60% of the flux to the K band, and along with the intermediate-age population it contributes more than 40% even to the blue continuum. Test cases show that it is not possible to reproduce the broad features of the continuum and, in particular, the depth of the Ca II K line by suppressing the older population, even by assuming a higher metal content. Hence, in most of the M82-like starburst galaxies, the K -band luminosity can be used as an estimate of stellar mass. However, when the birthrate parameter exceeds the average value of our sample galaxies ($\simeq 5$), the young populations start contributing a significant fraction to the NIR luminosity. This should be taken into account when trying to determine, from the rest-frame optical-NIR luminosity, the mass of the old component in high-redshift galaxies, where at a given SFR the birthrate parameter is likely to be larger.

The regions with ongoing star formation have systematically higher extinction than the older populations: $A_V(\text{old})/A_V(\text{young}) = 0.43 \pm 0.13$. The fact that the continuum of starburst nuclei is mainly contributed by the old population makes this result identical to that obtained by Calzetti et al. (1994), who found $A_V(\text{continuum})/A_V(\text{emission line}) = 0.50$. It was not possible to reliably determine the extinction of the intermediate-age population as a result of the small base wavelength over which this population dominates, if at all, in the sample nuclei.

The decomposition of the observed spectra into spectra of individual populations allowed us to determine the underlying absorption EWs for Balmer lines. The resulting mean value for H α is $1.6 \pm 0.3 \text{ \AA}$, and it is around $2.4 \pm 0.8 \text{ \AA}$ for the rest of the Balmer lines, where the errors represent the real variations from galaxy to galaxy and are not due to measurement errors. Hence, in a given galaxy, the correction to H α is always smaller than that for the other three lines. These values are improvements over the values suggested by McCall et al. (1985), who obtained the correction by forcing it to be the same for the first three Balmer lines. As expected, the value of $1.9 \pm 0.3 \text{ \AA}$ that was obtained by McCall et al. is intermediate between those of H α and the rest of the Balmer lines. The continuum from the old population plays an important role in reducing (or diluting) the observed emission EWs below the values

expected for a purely young burst. We find that the mean dilution factors for $H\alpha$ and $H\beta$ are 4.7 ± 1.9 and 3.2 ± 1.2 , respectively.

We thank Bianca Poggianti, Pasquale Panuzzo, Alberto Franceschini, and Roberto Terlevich for thoughtful discussions. We also thank the referee for several useful comments, which

have enabled us to improve the original manuscript. This work was partly supported by the CONACyT projects 39714-F, 36547-E, and J37680-E. A. B. thanks INAOE for its kind hospitality during his visits. This research has made use of the NASA/IPAC Extragalactic Database, which is operated by the Jet Propulsion Laboratory, California Institute of Technology, under contract with the National Aeronautics and Space Administration.

REFERENCES

- Balzano, V. A. 1983, *ApJ*, 268, 602
 Bressan, A., Granato, G. L., & Silva, L. 1998, *A&A*, 332, 135
 Bruzual A., G. 1983, *ApJ*, 273, 105
 Burstein, D., Haynes, M. P., & Faber, S. M. 1991, *Nature*, 353, 515
 Calzetti, D., Kinney, A. L., & Storchi-Bergmann, T. 1994, *ApJ*, 429, 582
 Cardelli, J. A., Clayton, G. C., & Mathis, J. S. 1989, *ApJ*, 345, 245
 Charlot, S., & Fall, S. M. 2000, *ApJ*, 539, 718
 Cizdziel, P. J., Wynn-Williams, C. G., & Becklin, E. E. 1985, *AJ*, 90, 731
 Devereux, N. 1987, *ApJ*, 323, 91
 ———. 1989, *ApJ*, 346, 126
 Evans, R. 1994, *MNRAS*, 266, 511
 Fanelli, M. N., O'Connell, R. W., & Thuan, T. X. 1988, *ApJ*, 334, 665
 Ferland, G. J. 1996, *Hazy: A Brief Introduction to CLOUDY*, Dept. of Physics and Astronomy Internal Rep. (Lexington: Univ. Kentucky
 Förster-Schreiber, N. M., Sauvage, M., Charmandaris, V., Laurent, O., Gallais, P., Mirabel, I. F., & Vigroux, L. 2003, *A&A*, 399, 833
 Granato, G. L., Silva, L., Bressan, A., Lacey, C. G., Baugh, C. M., Cole, S., & Frenk, C. S. 2001, *Ap&SSS*, 277, 79
 Gu, Q. S., Huang, J. H., de Diego, J. A., Dultzin-Hacyan, D., Lei, S. J., & Benítez, E. 2001, *A&A*, 374, 932
 Helou, G., Khan, I. R., Malek, L., & Boehmer, L. 1988, *ApJS*, 68, 151
 Holweger, H. 2001, in *AIP Conf. Proc.* 598, *Solar and Galactic Composition*, ed. R. F. Wimmer-Schweingruber (New York: AIP), 23
 Ingber, L. 1989, *Math. Comput. Mod.*, 12, 967
 Jacoby, G. H., Hunter, D. A., & Christian, C. A. 1984, *ApJS*, 56, 257
 Kennicutt, R. C., Jr. 1992, *ApJ*, 388, 310
 Kennicutt, R. C., Jr., Tamblyn, P., & Congdon, C. W. 1994, *ApJ*, 435, 22
 Kim, D.-C., Sanders, D. B., Veilleux, S., Mazzarella, J. M., & Soifer, B. T. 1995, *ApJS*, 98, 129
 Kurucz, R. L. 1993, *Kurucz CD-ROM 13, Atmosphere Models* (Cambridge: SAO)
- Lançon, A., Goldader, J. D., Leitherer, C., & González-Delgado, R. 2001, *ApJ*, 552, 150
 Leitherer, C., et al. 1999, *ApJS*, 123, 3
 McCall, M. L., Rybski, P. M., & Shields, G. A. 1985, *ApJS*, 57, 1
 O'Connell, R. W., Gallagher, J. S., Hunter, D. A., & Colley, W. N. 1995, *ApJ*, 446, L1
 O'Connell, R. W., & Mangano, J. J. 1978, *ApJ*, 221, 62
 Osterbrock, D. E. 1989, *Astrophysics of Gaseous Nebulae and Active Galactic Nuclei* (Mill Valley: University Science)
 Panuzzo, P., Bressan, A., Granato, G. L., Silva, L., & Danese, L. 2003, *A&A*, 409, 99
 Pérez-González, P. G., et al. 2003, *MNRAS*, 338, 525
 Poggianti, B. M., Bressan, A., & Franceschini, A. 2001, *ApJ*, 550, 195
 Prugniel, P., & Héraudeau, P. 1998, *A&AS*, 128, 299
 Rieke, G. H., Lebofsky, M. J., Thompson, R. I., Low, F. J., & Tokunaga, A. T. 1980, *ApJ*, 238, 24
 Rieke, G. H., Loken, K., Rieke, M. J., & Tamblyn, P. 1993, *ApJ*, 412, 99
 Rodríguez-Merino, L. H., Chavez, M., Bertone, E., & Buzzoni, A. 2003, in *ASP Conf. Ser.* 297, *Star Formation through Time*, ed. E. Pérez, R. M. González Delgado, & G. Tenorio-Tagle (San Francisco: ASP), 237
 Rosa-González, D., Terlevich, E., & Terlevich, R. 2002, *MNRAS*, 332, 283
 Sadler, E. M., Rich, R. M., & Terndrup, D. M. 1996, *AJ*, 112, 171
 Silva, L., Granato, G. L., Bressan, A., & Danese, L. 1998, *ApJ*, 509, 103
 Tully, R. B. 1988, *The Nearby Galaxies Catalog* (Cambridge: Cambridge Univ. Press)
 Veilleux, S., Kim, D.-C., Sanders, D. B., Mazzarella, J. M., & Soifer, B. T. 1995, *ApJS*, 98, 171
 Walter, F., Weiss, A., & Scoville, N. 2002, *ApJ*, 580, L21
 Weedman, D. W., Feldman, F. R., Balzano, V. A., Ramsey, L. W., Sramek, R. A., & Wu, C.-C. 1981, *ApJ*, 248, 105